European Journal of Mechanics / B Fluids 117 (2026) 204450

Contents lists available at ScienceDirect

European Journal of Mechanics / B Fluids

journal homepage: www.elsevier.com/locate/ejmflu

# Analysis of compliant tube properties and operating conditions in a Liebau pump☆

Manuel Rubio [a,*], Francisco Castro-Ruiz [a], José Sierra-Pallares [a], César Barrios-Collado [a], Joaquín Anatol [b]

[a] Departamento de Ingeniería Energética y Fluidomecanica & ITAP, Universidad de Valladolid, Paseo del Cauce 59, 47011 Valladolid, Spain
[b] Departamento de Ingeniería Energética, Universidad Politécnica de Madrid, C/ José Gutiérrez Abascal 2, 28006, Madrid, Spain

ARTICLE INFO

*Keywords:*
Valveless pumping
Liebau effect
Asymmetric pumping

ABSTRACT

This study examines asymmetric pumping in Liebau pumps, a type of valveless pump that generates unidirectional flow through the periodic compression of a flexible (compliant) tube. This pumping has applications in biomedical devices, microfluidics, and organ support. We investigate how the properties of the compliant tube and the operating conditions affect the pump performance, using dimensionless parameters. Experiments were performed with different configurations, varying the tube material (latex and rubber) and the fluid (water and water–glycerine mixture).

The results indicate that the flow rate and resonant period depend on the stiffness of the tube and the viscous effects. It was observed that for small values of the Womersley number ($Wo^2$), viscous effects significantly reduce the flow rate. In contrast, for large Womersley values, the semiempirical models previously proposed adequately predict the experimental behaviour. Effects such as the compliant tube depression, which were not accounted for in previous models, were also found to influence performance. This work extends the analysis of this type of pump to unexplored conditions, with the aim of expanding knowledge and enabling the use of Liebau pumps in real-world applications.

## 1. Introduction

The Liebau effect refers to a mechanism of valveless pumping, generating unidirectional fluid flow through periodic compression of a flexible (compliant) tube without the use of valves [1]. Its practical and potential applications are found both in biological and engineering contexts. The Liebau effect is considered a fundamental principle for flow generation in the early embryonic heart, which functions as a tubular, valveless pump before the development of conventional valves. Studies indicate the form (straight vs. kinked/twisted tubes) of the embryonic heart may significantly influence pumping efficiency via this mechanism [2]. A valveless pumping system requires specific structural and material characteristics, such as tubing with spatially varying elastic properties and a mechanical actuator (commonly referred to as a pincher), which is critical for transferring energy to the fluid [3]. For pumping to be effective, the compliant section of the tube must be compressed at a particular frequency, which is determined by the geometric configuration of the system. The Liebau effect encompasses two primary modes of pumping: asymmetric and impedance. Asymmetric volumetric pumping occurs when compression is applied at the mid-transversal plane of the compliant tube. At the same time, the surrounding circuit exhibits asymmetry — this can arise from variations in the length, diameter, or material composition of the adjoining rigid tubes. Additionally, some volumetric pumping of the same kind can be obtained even when the pincher is out of the mid-plane [4]. Impedance pumping, on the other hand, is a kind of pumping produced by wave reflections, and it is only enters into play when the compression is performed at a transversal plane different from the mid-plane. In both mechanisms, the flow rate generated is not linearly proportional to the actuation frequency. The frequency that yields the maximum flow rate is referred to as the resonant frequency.

The physics of Liebau effect pumping is complex because multiple variables are involved, and each has an impact on flow direction and amplitude [5]. Since its discovery, several authors have sought to gain a deeper understanding of this phenomenon and test its applicability in various fields. Impedance pumping has been the most studied and analysed mechanism by different authors since the Liebau phenomenon was first observed. This pumping mechanism has been investigated experimentally [5–8] and by numerical and analytical models [4,9,10].

☆ This article is part of a Special issue entitled: 'SFMC25 Adv. Fluid Mech.' published in European Journal of Mechanics / B Fluids.

* Corresponding author.
*E-mail address:* manuel.rubio@uva.es (M. Rubio).

https://doi.org/10.1016/j.euromechflu.2025.204450

Available online 26 December 2025

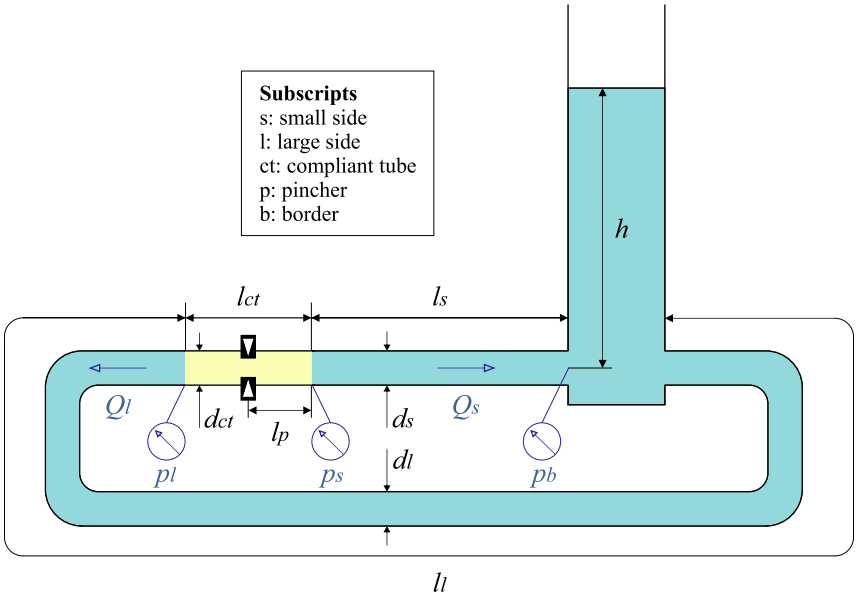


**Fig. 1.** Diagram of the experimental facility.

Asymmetric pumping has been less studied than impedance pumping; there are also experimental investigations [11–13], and numerical and analytical models [14–16].

Takagi and Saijo [13] experimentally and analytically analysed the behaviour of an asymmetric pump. They observed that in this pumping mode, the velocity amplitude is different in the long and small tubes. In addition, they developed a model consisting of ordinary differential equations that could predict the pumping effect, which was validated using experimental data. Later, Takagi and Takahashi [15] continued this work, maintaining the circuit but pressurising the tanks.

Propst [14] described the theoretical foundations of asymmetric pumping. He considered different circuit configurations consisting of tanks connected by rigid tubes. For that purpose, Propst used a time-averaged energy equation. He stated that pumping is caused by the difference in kinetic energy between the two tube sections of the two branches. The difference in kinetic energy was attributed to the varying loss constants in tube-to-tank couplings and vice versa. Jung and Kim [17] proposed an asymmetric valveless pumping model in an open system consisting of two tanks connected with a horizontal tube. They used an energy conservation model applied to consecutive control volumes, denoted as compartments, in one or more of which the mechanical actuation on a piece of elastic tube could be modelled. They studied the appearance of a net unidirectional flow when the compartment was excited, emulating an elastic tube. Furthermore, they confirmed that the direction and magnitude of the net flow depend on the pinching frequency and established that the resonant frequency is the optimum to work with asymmetric pumps. Finally, studies of Liebau pumping are discussed that refer to mixed systems combining impedance pumping and asymmetric pumping. There is the experimental work of Liebau himself [1] and other experimental work [4,18,19].

However, research on simplified models of the Liebau phenomenon is more scarce. Simplified models can be used in pump performance optimisation due to their low computational cost and reliability. In this regard, the pioneering work of Rubio et al. [4,16] provides an in-depth description of asymmetric pumping, offering a simple yet effective semiempirical mathematical model that can predict the resonant frequency and flow rates. The model is based on applying the principles of conservation of momentum to the rigid tubes. It is also difficult to find studies where the length of the rigid tubing is of the same magnitude or longer than the compliant tube.

Liebau effect pumps are simple pumping devices, with no complex parts or internal geometries. These characteristics make them well-suited for integration when a non-invasive, space-saving, and low-cost pumping system is required. For these reasons, valveless pumping with Liebau effect pumps becomes particularly interesting in applications such as nanotechnology [20], chemical analysis and control [21], micro-engineering [22], cooling systems [8], and biomedical engineering [23]. In the latter field, the proposed Liebau effect pumps are particularly suitable for many applications, as they operate with small excitations. This condition may be necessary in confined environments [9], highlighting their potential for use both as intra-corporeal assistance devices and extracorporeal assistance devices. Recently, Sarvazyan [24] conducted an extensive compilation on the state of the art in the construction of Liebau effect pumps and their potential biomedical applications.

Although a significant number of papers address the Liebau effect and its applications, little research has been conducted on the importance of the building materials of the compliant tube in the pump and the impact of fluid viscosity on pump behaviour. This knowledge is essential for potential applications, particularly in the fields of medicine and microfluidics, where robust and biocompatible materials are required and viscosity forces become significant.

This paper addresses those questions in detail, providing experimental data, and a physical explanation of the phenomena underlying these effects. The pumping performance is analysed for different fluid and compliant tube properties, as well as for different operating conditions. Furthermore, the limits of application of the semiempirical model previously developed by this group [4,16] are tested.

## 2. Materials and methods

### 2.1. Experimental test rig

The experimental setup, shown in Fig. 1, mirrors the configuration examined in [4]. The setup consists of a closed hydraulic circuit that includes an atmospheric tank and a Liebau pump. The pump comprises two rigid tubes flanking a compliant tube, to which periodic compression is directly applied.

To establish geometric asymmetry within the facility, the two rigid tubes have been constructed with differing lengths. For ease of distinction, the small tube is assigned the subscript $s$, while the subscript $l$

**Table 1**
Experimental configurations tested in this work.

| Parameter | Conf 1 | Conf 2 | Conf 3 | Conf 4 |
|---|---|---|---|---|
| Fluid | Water | Water | Water | Water–Glycerine |
| Compliant tube material | Latex | Rubber | Latex | Latex |
| $l_t = l_s + l_l$ | 7.1 m | 7.1 m | 37.1 m | 7.1 m |
| $Wo^2$ | 82–201 | 82–171 | 15–38 | 7–18 |
| $\hat{G}$ | 42–251 | 92–400 | 42–251 | 40–241 |

denotes the large tube. Both tubes have an identical inner diameter of $d_s = d_l = 20$ mm. The parameter that quantifies the asymmetry between these conduits is $\Lambda = \frac{l_l A_s}{l_s A_l}$, where $A$ represents the area of the tube. Throughout the configurations examined in this study, $\Lambda$ has been consistently maintained at a value of 5.3. Table 1 in Section 2.3 presents the lengths of the rigid tubes for each configuration.

In the experiments involving the compliant tube, two distinct materials, namely Latex and Rubber, have been evaluated. Both materials have been characterised previously, using both experimental and numerical methods [25], possessing shear moduli of $G = 0.37$ MPa and $G = 0.59$ MPa, respectively. These materials maintain identical dimensions, with a inner diameter of $d_{ct} = 20$ mm and a length of $l_{ct} = 100$ mm. The actuator, designed to apply compression to the compliant tube, consists of two resin prisms [4], each with a width of 20 mm, that traverse the length of the tube. These prisms exert symmetrical compression in relation to the transverse plane of the tube. The actuator design facilitates axial adjustments along the axis of symmetry of the compliant tube, represented by $l_p$. The actuator's positioning is defined by the parameter $\beta = l_p/l_{ct}$. For this study, $\beta$ has a constant value of 0.5, ensuring the actuator is precisely situated at the tube's midpoint. The actuator's motion follows a quasi-square periodic signal with a period ($T$). The percentage of the cycle duration spent applying compression to the compliant tube is named the duty cycle ($\gamma$). Both can be set for each experiment.

The measuring instruments used were a bidirectional ultrasonic flowmeter (Sonotec Sonoflow CO.55/329H V2.0) placed in the large tube and three manometric pressure sensors (Keller PD-23), two of them placed at each end of the compliant tube ($p_s$ and $p_l$) and the other at the tank ($p_b$). $p_b$ results from the hydrostatic pressure in the tank and is considered not to vary significantly during an experiment, since the tank has a sufficiently large cross-section (rectangular section of 15 cm ×10 cm). The uncertainty is 2% for the flowmeter and 4% for the pressure gauges. The in-house-made acquisition system, based on Arduino Due™, has a data acquisition rate of 1 kHz. Water and a mixture of water and glycerine (35/65%(w/w)) are used, the latter with density $\rho = 1040$ kg/m$^3$ and viscosity $\mu = 0.011$ kg/m s at 25°C, measured with a HAAKE RheoStress RS80 rheometer.

### 2.2. Test parameters

The operating conditions at resonance of the Liebau pump are the period, $T_r$, the duty cycle, $\gamma$, and the net pumped flow rate, $Q_r$. We refer to resonant conditions as the values of the period and duty cycle for which the net pumped flow rate is maximum. The subscript $r$ is used to indicate resonant conditions.

The resonant net flow rate and period depend on the configuration and dimensions of the facility, the operation characteristics (pressure at the ends of the rigid tubes, $p_b$), the density and viscosity of the fluid, and the mechanical properties of the compliant tube, represented by the shear modulus $G$.

In [4], it was deduced that the maximum net flow rate ($Q_{ic}$) driven for a given set of ideal conditions and the period for such conditions ($T_{ic}$) are calculated according to the equations:

$$Q_{ic} = \sqrt{\frac{A_s p_b V_{ct}}{2\rho l_s}}$$
$$T_{ic} = \sqrt{\frac{2\rho V_{ct} l_s}{A_s p_b}} \tag{1}$$

where $V_{ct}$ is the inner volume of the compliant tube. Applying the dimensionless formulation proposed in [4], in which time is made dimensionless by $T_{ic}$, flow rates by $Q_{ic}$ and pressures by $p_b$, the following relationship is derived:

$$\left(\hat{T}_r, \hat{Q}_r\right) = \varphi\left(\Lambda, \beta, \hat{G}, W_0^2\right) \tag{2}$$

From now on, to distinguish between dimensional and dimensionless parameters, the latter will be highlighted with the caret symbol (ˆ). In contrast to [4], which employed $\hat{p}_m = p_m/p_b$, the present work adopts $\hat{G} = G/p_b$ instead. This modification was made because $p_m$ is an experimentally derived quantity, whereas $G$ represents an intrinsic mechanical property of the compliant tube. $Wo^2$ is the square of the Womersley number, which evaluates the importance of the viscous term:

$$Wo^2 = \frac{d^2\sqrt{\rho\,\Delta p}}{\mu\, l} \tag{3}$$

where $\rho$ and $\mu$ are the density and viscosity of the fluid, $d$ and $l$ are the diameter and length of the rigid tubes, and $\Delta p$ is the pressure difference between the ends of the tubes. The importance of the viscous term will be greater the smaller $Wo^2$. Additionally, $Wo^2$ takes the smallest values on the large side when the compliant tube is being filled ($\Delta p \approx p_b$). Therefore, its expression throughout this work will be

$$Wo^2 = \frac{d_l^2\sqrt{\rho\, p_b}}{\mu\, l_l} \tag{4}$$

The influence of the geometrical parameters $\Lambda$ and $\beta$ has already been studied in previous works when the viscous terms are subdominant, [4,16]. In this work, we study the influence of the viscous terms and the material of the compliant tube through the parameters $Wo^2$ and $\hat{G}$, respectively.

### 2.3. Experiments

Experiments have been conducted with four different configurations, as described in Table 1. For all the configurations $\Lambda = 5.3$ and $\beta = 0.5$. Configuration 1 is based on the results shown in [4], using the same fluid, compliant tube material, and a length of the rigid sections for which $Wo^2$ is high enough. Table 1 shows the range of $Wo^2$ and $\hat{G}$ for each configuration.

Configuration 2 is designed to explore a case with a higher value of $\hat{G}$, given that rubber is stiffer than latex. Configuration 3 focuses on lowering $Wo^2$ by enlarging the dimensions of both rigid tubes. Lastly, Configuration 4 also aims to decrease $Wo^2$ to levels similar to those in Configuration 3, but achieves this by using a fluid with greater viscosity.

To summarise, the value of $\hat{G}$ has been varied through $p_b$ by imposing different water heights on the tank and using two materials of different stiffness for the compliant tube. The value of the Womersley number $Wo^2$ has been modified through $p_b$, two fluids of different density and viscosity, and two total lengths of the tubes.

The range of $Wo^2$ and $\hat{G}$ is the result of four experimental series corresponding to four different heights (between 0.15 and 0.9 m) for each configuration. In each series, to determine the resonant period, a period sweep comprising 20 experiments was performed with a time increment ranging from 25 ms to 100 ms, depending on the configuration. For each period, three duty cycles (0.25, 0.35, and 0.45) were tested, and the resonant cycle was chosen as the one with the highest net flow rate. The total number of experiments per configuration was 240.

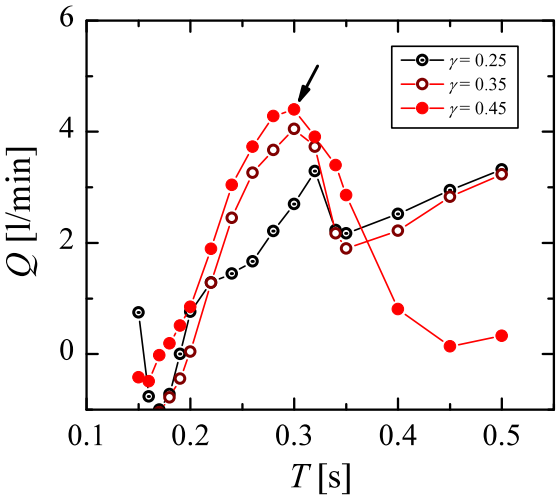


**Fig. 2.** Experimental sweep of net flow rate ($Q$) as a function of period ($T$) for different duty cycles. An arrow indicates the resonant conditions. The parameters of the experiment are $\Lambda = 5.3$, $\beta = 0.5$, $\hat{G} = 94$, $Wo^2 = 134$.

#### 2.3.1. Experimental procedure

An example of the experimental procedure to obtain the resonant period and net flow rate is shown in Fig. 2. Configuration 1 is used with $h = 0.4$ m, and with values of $Wo^2 = 134$ and $\hat{G} = 94$. The maximum flow value determines the resonant conditions ($T_r = 0.3$ s and $Q_r = 4.4$ l/min). This case corresponds to a duty cycle $\gamma = 0.45$.

Keeping the same configuration, three more heights are tested, and the results shown in Fig. 3 (left) are obtained. From these data, the resonant conditions are determined for each height, which are shown in Fig. 3-right. The last figure illustrates that the values of $h$ (and therefore, $p_b = \rho g h$) do not affect the resonant period, but they do influence the driven net flow rate.

Hereafter, to generalise the results, they will be presented in a dimensionless form.

## 3. Results

The results is divided into two sections. The first examines the influence of the parameters $\hat{G}$ and $Wo^2$ from the tests conducted. The second section compares the results with the model of Rubio et al. [4].

### 3.1. Analysis of $\hat{G}$ and $Wo^2$ influence

The parameter $\hat{G} = G/p_b$ is calculated from the shear modulus of the compliant tube, $G$, and the pressure of the bottom of the tank, $p_b$. To study its influence on the pump performance, we modify its value in two different ways: through a variation in the fluid height of the tank, $h$, which alters $p_b = \rho g h$, and through the study of two compliant tubes with different shear moduli. The values of $\hat{G}$ will be higher for the experiments with lower fluid tank heights and when the compliant tube is stiffer, as is the case with the Rubber tube. These results are presented in Fig. 4.

Period $\hat{T}_r$ decreases as the value of $\hat{G}$ increases (Fig. 4-left), with a similar trend for both materials. With respect to the resonant net flow rate $\hat{Q}_r$, (Fig. 4-right), the experiments take values close to those provided by the model of Rubio et al. [4], except for $\hat{G} > 200$ for both latex and rubber tube, where the flow rate is higher than expected. The reasons of this will be discussed at the end of Section 3.2.

The parameter $Wo^2 = \frac{d_i^2\sqrt{\rho\, p_b}}{\mu\, l_l}$ evaluates the importance of the viscous term in the fluid motion in rigid tubes. If $Wo^2$ is high enough, the viscous term is subdominant. In the experiments shown in Fig. 4, this parameter is always higher than 80, so the viscosity term has no influence. The next step in this study will be to evaluate this parameter experimentally. $Wo^2$ has been modified in two ways: by varying the length of the larger tube and by using two fluids of different viscosity and density.

These results are shown in Fig. 5. The experiments with $Wo^2$ between 80 and 200 (red solid symbols) correspond to a facility with a total length of 7.1 m and water as working fluid. These results are compared with those of a water–glycerine mixture as working fluid (blue hollow symbols) and with those of a facility of longer length ($l_t = 37.1$ m, green solid symbols). In the latter two cases, $Wo^2$ is reduced to values between 7 and 38. Analysing the resonant period with respect to $\hat{G}$ (Fig. 5-left), it can be seen that, for the range studied, the period varies relatively little between experiments with the same $\hat{G}$. Regarding Fig. 5-right, in the experiments with low $Wo^2$, the net flow rate is significantly lower, with this reduction being larger for low $\hat{G}$. Moreover, for $\hat{G} < 200$, the net flow rate is found to be lower than that obtained by the model described in Rubio et al. [4]. This model is valid when the viscous term is negligible, so it is expected to agree only with experiments with $Wo^2$ high enough.

The minimum $Wo^2$ analysed is around 10; thus, it is dubious whether the viscous term is subdominant or not. To check if it is exerting an effect, we will use the expression below applied to the large rigid tube. This expression was derived in [4]

$$\frac{\partial \hat{Q}_l}{\partial \hat{t}} = \frac{2}{\Lambda}\Delta\hat{p}_l \tag{5}$$

In this expression, valid only for high enough $Wo^2$, the derivative of the instantaneous flow rate with respect to time is directly proportional to $\Delta\hat{p}_l = (p_{ct} - p_b)/p_b$, which represents the pressure difference between the ends of the large tube. The results for $Wo^2 = 171$ and $\hat{G} = 58$ are presented in Fig. 6-left. In that experiment, the slope of the flow curve with respect to time is positive when the pressure difference is positive, and the opposite happens when the pressure difference is negative. This does not happen in an experiment with lower $Wo^2$ (Fig. 6-right), so Eq. (5) would not be fulfilled, possibly because the viscosity term is no longer subdominant.

### 3.2. Comparison with the model of Rubio et al. [4]

In this section, the experiments will be compared with the analytical model published in [4]. This semi-empirical model enables the determination of both the resonant net flow rate and the period by integrating the evolution of the compliant tube's volume between two states. When the tube's volume exceeds its resting value, its walls are stretched, resulting in an internal overpressure of magnitude $\hat{p}_m$. Conversely, when the volume falls below the resting level, the internal pressure approximates ambient conditions. Therefore, the parameter that characterises the mechanical behaviour of the elastic tube material is $\hat{p}_m$ instead of $\hat{G}$. Therefore, this parameter will be used in this section to compare the results with those of the model. $p_m = p_m/p_b$ is calculated from the average pressure in the compliant tube when it is stretched, $p_m$. The calculation of $p_m$ is addressed by fitting the time evolution of pressure in the compliant tube to a step function between the values of zero and $p_m$ [4]. An example of this fit is shown in Fig. 9.

As with $\hat{G}$, the values of $\hat{p}_m$ will be higher for experiments with lower tank heights and when the compliant tube is stiffer, as is the case with the rubber tube. In this section, we will analyse those experiments where the viscous term is negligible, which will be the same as those shown in Fig. 4 (latex and rubber). For example, Fig. 7 illustrates the dimensionless period sweep from experiments conducted with configuration 1. It is compared with the model results, which are represented in open symbols. It can be seen how the experimental results for $\hat{p}_m < 3$ agree correctly with the model results. The mismatch for $\hat{p}_m = 5.1$ will be analysed later.

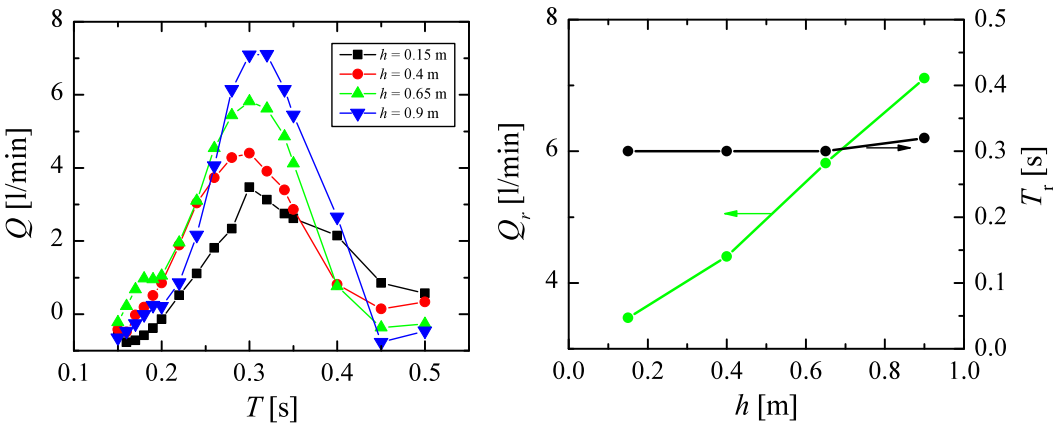


**Fig. 3.** (left) Experimental sweep of net flow rate ($Q$) as a function of period ($T$) for different heights; (right) resonant net flow rate ($Q_r$) and period ($T_r$) as a function of height ($h$). The parameters are as marked in Table 1-conf. 1.

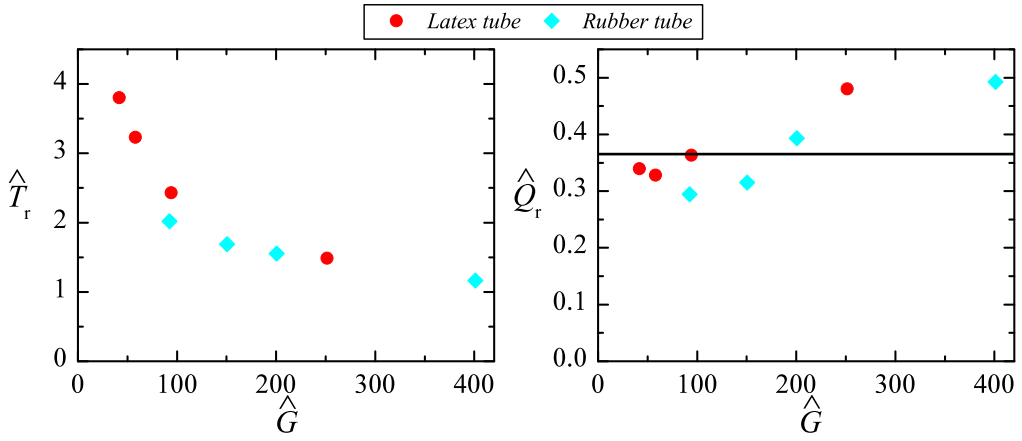


**Fig. 4.** (Left) resonant period ($\hat{T}_r$) and (right) net flow rate ($\hat{Q}_r$) as a function of $\hat{G}$ for configurations 1 (red circles) and 2 (cyan blue diamonds). The black line indicates the results of the Rubio et al. model [4] for those conditions.

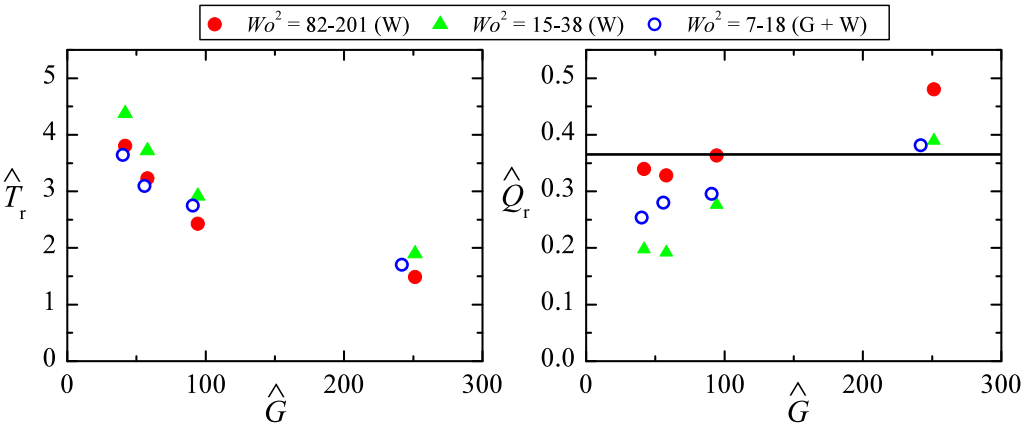


**Fig. 5.** (Left) resonant period ($\hat{T}_r$) and (right) net flow rate ($\hat{Q}_r$) as a function of $\hat{G}$ for configurations 1 (red solid circles), 3 (green solid triangles) and 4 (blue open circles).

If we combine the previous results with those of configuration 2 (rubber tube), we obtain Fig. 8, which also includes the results of the model for the same configuration. The period $\hat{T}_r$ decreases as the value of $\hat{p}_m$ increases with a similar trend to that predicted by the model (Fig. 8-left). However, for values higher than 2.5, the experimental period obtained is lower than the one provided by the model. With respect to the flow rate $\hat{Q}_r$, (Fig. 8-right), the experiments take values close to those provided by the model, except for the case of a lower $\hat{p}_b$ for both the latex and the rubber tube. We will now analyse what is happening in this limit, and why the pump performance is better.

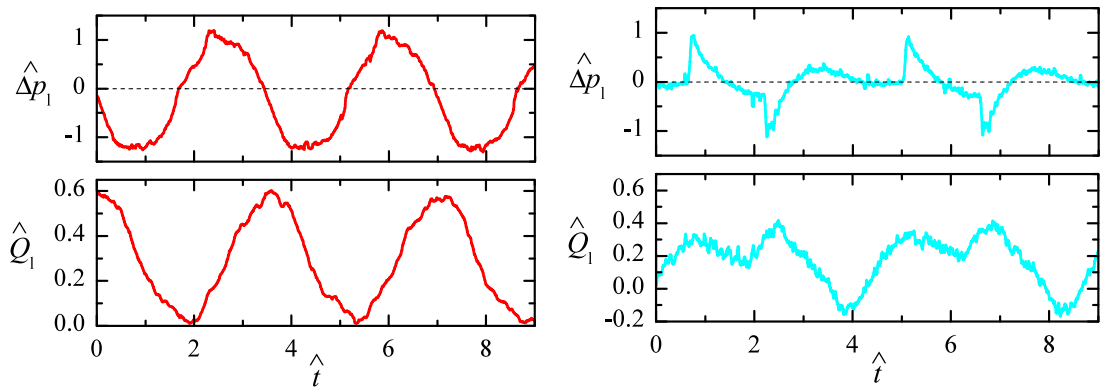


**Fig. 6.** Temporal evolution of $\Delta\hat{p}_l$ and $\hat{Q}_l$ for (left) $\Lambda = 5.3, \beta = 0.5, \hat{G} = 58$ and $Wo^2 = 171$; (right) $\Lambda = 5.3, \beta = 0.5, \hat{G} = 58$ and $Wo^2 = 32$.

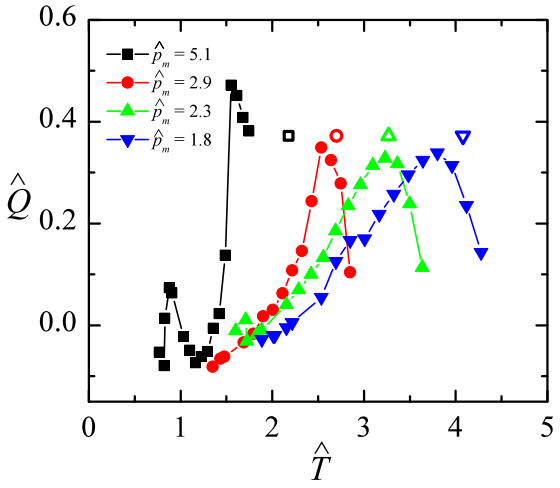


**Fig. 7.** Experimental sweep of net flow rate ($\hat{Q}$) as a function of period ($\hat{T}$) for different values of $\hat{p}_m$. Open symbols correspond to the results of Rubio et al. in [4]. The parameters are as marked in Table 1 (configuration 1).

To analyse what is happening, the evolution of the pressure difference between the ends of the large rube and its instantaneous flow rate is analysed in two latex tube experiments. For the case of $\hat{p}_m = 2.2$ (Fig. 9-left), the model adequately predicts both the period and the flow rate. This is also seen in the agreement between the model and the experimental instantaneous flow signal on the large tube ($Q_l$). However, for the case of $\hat{p}_m = 5.1$ (Fig. 9-right) there are discrepancies. The experimental period is 33% lower, as a result of the depression in the compliant tube (indicated by arrows). This depression, which is not accounted for in the model, causes the instantaneous flow rate to reduce more rapidly and shortens the cycle. As a result of the shorter period, the driven flow rate is higher than that provided by the model. The value of $\hat{G}$ in this experiment is 251, and this is also observed in the experiment with the highest $\hat{G}$ with the rubber compliant tube. $h$ is 0.15 m in both experiments, the minimum value studied.

The depression occurs when the compliant tube collapses. In those moments, the compliant tube is almost entirely squeezed, and the fluid is being emptied from the tubes to the tanks. Inertial terms of the momentum equation are responsible for this behaviour. The depression occurs earlier in the small tube than in the large tube because this side of the compliant tube is emptied earlier. Furthermore, it can be observed that the depression in the large tube disappears at the instant when the instantaneous flow rate becomes zero, thereby eliminating the fluid's inertia.

The model presented in [4] is notable for its simplicity. Still, in this work, for the experiments performed, it has been shown that it only adequately predicts the resonant conditions for sufficiently high $Wo^2$ and for a range of $\hat{p}_m$ (or $\hat{G}$). To obtain accurate results in these configurations, it is necessary to resort to more comprehensive models, such as fluid–structure simulations. These models should at least include the compliance of the tube section, as it plays a pivotal role in capturing the systems mechanical behaviour and pressure dynamics

## 4. Conclusions

This work has analysed how the mechanical properties of the compliant tube and the operating conditions affect the performance of a Liebau pump. For this purpose, experiments have been conducted with various configurations, varying the tube material (latex and rubber), the fluid (water and a water–glycerine mixture), and the dimensions of the rigid tubes.

Firstly, the influence of the stiffness of the compliant tube in the absence of viscous effects has been analysed through the dimensionless parameter $\hat{G}$. The results show that its behaviour is similar to that observed when $\hat{p}_m$ is used as a parameter. $\hat{G}$ has a direct impact on the resonant period. The higher the stiffness, the smaller the dimensionless resonant period. Regarding the net flow rate, the model described in [4] suggests that the flow rate should not depend on the stiffness of the compliant tube. This behaviour has been observed in most experiments, except in cases where the material exhibits the highest $\hat{G}$ value, leading to a flow rate that exceeds expectations. In these experiments, a phenomenon not previously considered in models has been identified: the depression that occurs when the compliant tube collapses. This depression shortens the pumping cycle and increases the net flow rate, thereby improving performance.

Second, regarding the importance of viscous effects, the Womersley number has been swept for three different configurations. As expected, when the value of this number is low, the net flow rate is significantly reduced, which limits the pump performance. In contrast, the period is hardly affected. This happens both when $Wo^2$ is reduced by increasing the tube lengths and when the viscosity of the working fluid is higher.

Finally, the results have been compared with the numerical model described in [4]. This model adequately predicts the pump behaviour under conditions where viscous effects are negligible. However, under low $Wo^2$ or high $\hat{G}$ conditions, deviations are observed. To predict pump performance under these conditions, it would be necessary to resort to more comprehensive models, such as fluid–structure simulations of at least the compliant tube.

This study has expanded the analysis of Liebau pumps, extending their evaluation to operating conditions that have not been previously considered in the literature. By exploring new operating scenarios, the aim is to analyse their viability in specific applications, such as biomedical engineering or microfluidics.

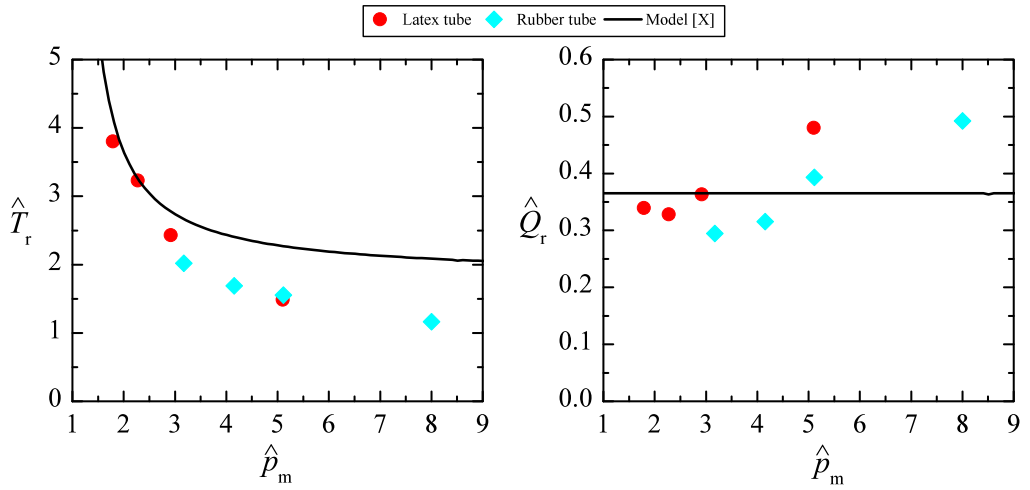


**Fig. 8.** (Left) resonant period ($\hat{T}_r$) and (right) net flow rate ($\hat{Q}_r$) as a function of $\hat{G}$ for different compliant tubes. In red symbols, the results for the latex-compliant tube; in blue, for the rubber-compliant tube; and in a black line, the results of the model [4].

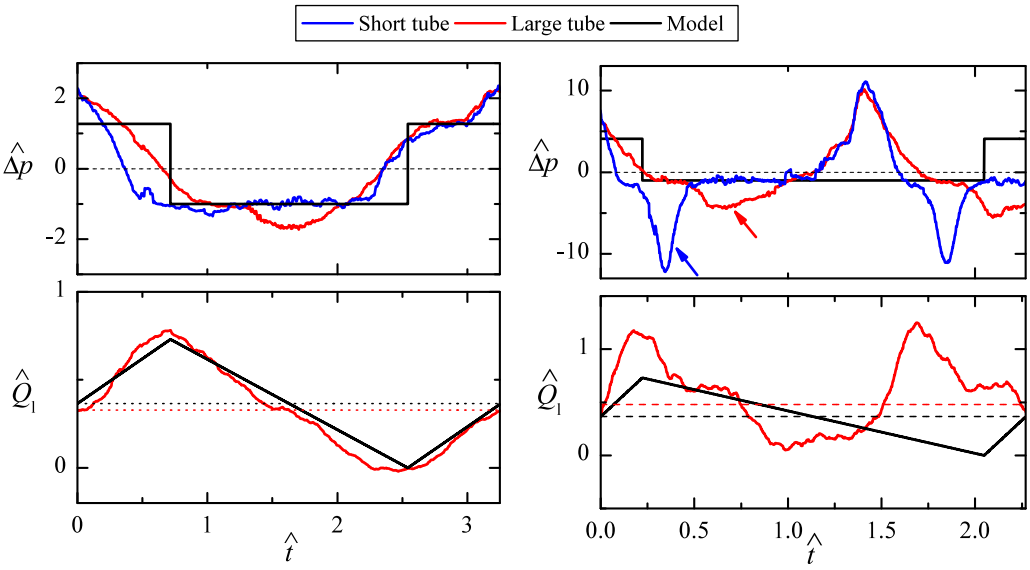


**Fig. 9.** Time evolution of $\Delta\hat{p}_l$, $\Delta\hat{p}_s$ and $\hat{Q}_l$ for $p_m = 2.2, Wo^2 = 171$ (on the left, both plots) $p_m = 5.1$, $Wo^2 = 82$ (on the right). In blue, the data for the small side, in red, the data for the large side, and in black, the model results. The horizontal lines of the flow graphs represent the experimental (red) and numerical (black) net flow rate. (For interpretation of the references to colour in this figure legend, the reader is referred to the web version of this article.)

## CRediT authorship contribution statement

**Manuel Rubio:** Writing – review & editing, Writing – original draft, Visualization, Validation, Supervision, Project administration, Methodology, Investigation, Formal analysis, Data curation, Conceptualization. **Francisco Castro-Ruiz:** Writing – review & editing, Writing – original draft, Methodology, Conceptualization. **José Sierra-Pallares:** Writing – review & editing, Writing – original draft, Methodology, Investigation. **César Barrios-Collado:** Writing – review & editing, Validation, Investigation, Formal analysis. **Joaquín Anatol:** Writing – review & editing, Writing – original draft, Methodology, Investigation, Formal analysis.

## Declaration of competing interest

The authors declare that they have no known competing financial interests or personal relationships that could have appeared to influence the work reported in this paper.

## Acknowledgements

The authors would like to thank the Junta de Castilla y León for funding this work as part of the programme "Subvenciones del programa de apoyo a proyectos de investigación financiados por fondos FEDER", project number VA182P20.

## Data availability

Data will be made available on request.

## References

[1] G. Liebau, Über ein ventilloses pumpprinzip, Naturwissenschaften 41 (1954) 327.
[2] F. Hiermeier, J. Männer, Kinking and torsion can significantly improve the efficiency of valveless pumping in periodically compressed tubular conduits. Implications for understanding of the form-function relationship of embryonic heart tubes, J. Cardiovasc. Dev. Dis. 4 (4) (2017).
[3] T. Kenner, Biological asymmetry and cardiovascular blood transport, Cardiovasc. Eng. 4 (2004) 209–218.

[4] M. Rubio, F. Castro-Ruiz, J. Sierra-Pallares, C. Barrios-Collado, J. Anatol, Modeling Liebau pumping under resonant conditions, Phys. Fluids 37 (2025) 077175.
[5] C. Manopoulos, S. Tsangaris, D. Mathioulakis, Net flow generation in closed-loop valveless pumping, Proc. Inst. Mech. Eng. C 234 (2020) 2126–2142.
[6] R. Davtyan, N.A. Sarvazyan, Output of a valveless Liebau pump with biologically relevant vessel properties and compression frequencies, Sci. Rep. 11 (2021) 1–10.
[7] A.I. Hickerson, D. Rinderknecht, M. Gharib, Experimental study of the behavior of a valveless impedance pump, Exp. Fluids 38 (2005) 534–540.
[8] C.Y. Wen, S.J. Yeh, K.P. Leong, W.S. Kuo, H. Lin, Application of a valveless impedance pump in a liquid cooling system, IEEE Trans. Compon. Packag. Manuf. Technol. 3 (2013) 783–791.
[9] L. Loumes, I. Avrahami, M. Gharib, Resonant pumping in a multilayer impedance pump, Phys. Fluids 20 (2008) 1–12.
[10] I. Avrahami, M. Gharib, Computational studies of resonance wave pumping in compliant tubes, J. Fluid Mech. 608 (2008) 139–160.
[11] J. Anatol, M. García-Díaz, C. Barrios-Collado, J. Moneo-Fernández, M. Horvath, M. Parra-Santos, F. Castro-Ruiz, E. Roche, J. Sierra-Pallares, Experimental study of an asymmetric valveless pump to elucidate insights into strategies for pediatric extravascular flow augmentation, Sci. Rep. 12 (2022).
[12] J. Anatol, M. García-Díaz, C. Barrios-Collado, J. Moneo-Fernández, F. Castro-Ruiz, J. Sierra-Pallares, Experimental characterization of an asymmetric valveless pump based on soft robotics technology, Phys. Fluids 35 (2023).
[13] S. Takagi, T. Saijo, Study of a piston pump, without valves, Bull. JSME 26 (1983).
[14] G. Propst, Pumping effects in models of periodically forced flow configurations, Phys. D 217 (2006) 193–201.
[15] S. Takagi, K. Takahashi, Study of a piston pump without valves (2nd report), Bull. JSME 28 (1985).
[16] M. Rubio, J. Anatol, J. Sierra-Pallares, C. Barrios-Collado, F. Castro-Ruiz, A semi-empirical model to predict resonant conditions in valveless asymmetric pumping, J. Fluid Mech. 1007 (2025) A2.
[17] E.O. Jung, D.W. Kim, Valveless pumping in open tank system using energy conserving compartment model, Bull. Korean Math. Soc. 49 (2012) 961–987.
[18] N.M. Pahlevan, M. Gharib, In-vitro investigation of a potential wave pumping effect in human aorta, J. Biomech. 46 (2013) 2122–2129.
[19] J. Anatol, M. García-Díaz, C. Barrios-Collado, J. Moneo-Fernández, M. Rubio, F. Castro-Ruiz, J. Sierra-Pallares, An assessment of the suitability of a Liebau pump in biomedical applications, Phys. Fluids 36 (2024).
[20] H. Andersson, W. van der Wijngaart, P. Nilsson, P. Enoksson, G. Stemme, A valveless diffuser micropump for microfluidic analytical systems, Sensors Actuators B 72 (2001) 259–265.
[21] C.Y. Wen, C.H. Cheng, C.N. Jian, T.A. Nguyen, C.Y. Hsu, Y.R. Su, A valveless micro impedance pump driven by PZT actuation, Mater. Sci. Forum 505–507 (2006) 127–132.
[22] D. Rinderknecht, A.I. Hickerson, M. Gharib, A valveless micro impedance pump driven by electromagnetic actuation, J. Micromech. Microeng. 15 (2005) 861.
[23] J. Anatol, E. Vignali, E. Gasparotti, F. Castro-Ruiz, M. Rubio, C. Barrios-Collado, J. Sierra-Pallares, S. Celi, A novel valveless pulsatile flow pump for extracorporeal blood circulation, Ann. Biomed. Eng. (2025).
[24] N. Sarvazyan, Building valveless impedance pumps from biological components: Progress and challenges, Front. Physiol. 12 (2022) 1–13.
[25] M. Rubio, J. Anatol, C. Barrios-Collado, M.A. Herrada, A simple technique for characterizing flexible materials using pressurized tubes, 2025, Preprint, https://uvadoc.uva.es/handle/10324/80377.